

LIMNOLOGY and OCEANOGRAPHY

Seasonal dynamics of internal waves governed by stratification stability and wind: Analysis of high-resolution observations from the Dead Sea

Ali Arnon , 1,2 Steve Brenner, John S. Selker, Isaac Gertman, Nadav G. Lensky 1,2

- ¹Water and Natural Resources Division, Geological Survey of Israel, Jerusalem, Israel
- ²Department of Geography and Environment, Bar Ilan University, Ramat Gan, Israel
- ³Biological and Ecological Engineering, Oregon State University, Corvallis, Oregon

Abstract

Internal waves in stratified lakes are affected by the seasonally varying stratification and the wind forcing. We studied the seasonal dynamics of internal waves by means of high-resolution observations and model simulations for the Dead Sea. A two-layer hydrostatic model provided high correlations between measured thermocline depth and the lake level oscillations. Seasonally, the amplitude of the thermocline fluctuations were anticorrelated with the density difference between the water layers; the largest fluctuations were observed when stratification was weak in spring/fall and moderate to weak fluctuations in mid-summer when stratification was fully developed. The surface and the internal waves propagated counterclockwise along the coasts at a speed of ~0.5 m s⁻¹. Power spectra of the observed wind as well as the measured and simulated lake level and thermocline depth show a pronounced diurnal period during summer, suggesting forcing by the diurnally varying wind. During spring and fall, when the water column stability diminishes, a hint of longer wind periods appear in addition to the diurnal mode. Accordingly, the lake level and thermocline depth fluctuations respond at lower frequencies. In the fall, the longer wind periods are close to the lake's first vertical normal mode, suggesting that resonant amplification of the internal waves may explain the observed lower frequency response of the level and thermocline oscillations. Reduction of the stratification stability originating from anthropogenic water diversion over the past four decades, associated with lake level decline and salinity increase, have led to increases of internal waves amplitude and periods.

Background

Internal waves in lakes oscillate along the pycnocline with amplitudes of meters to tens of meters, depending on the basin shape and size as well as on the density stratification of the water column and on the external wind forcing (Wedderburn 1912; Mortimer 1953, 1993). The pycnocline oscillations are typically three orders of magnitudes larger than lake-surface oscillations, corresponding to the density contrast between layers ($\Delta \rho$, positive for stable layering) as compared to that of the air–water interface (Sirkes et al. 1997; Lemmin et al. 2005). The correlation between lake level offsets (d, positive upward) and thermocline depth oscillations (D, positive downward) can be approximated by a two layer model maintaining hydrostatic pressure as expressed by the following equation (Wyrtki and Kendall 1967):

Additional Supporting Information may be found in the online version of this article.

$$\frac{d}{D} = \frac{\Delta \rho}{\rho} \tag{1}$$

where ρ is the average density of the water column. Lakes experience seasonal variations of density stratification due to seasonal hydrological and heat cycles and due to interannual changes in density related to long-run processes, such as hydrological stress by climate or anthropogenic change (Williams 2001). These affect the internal wave characteristics according to the density ratio (Eq. 1). In this article, we investigate seasonal and interannual changes in the density stratification and their influence on the nature of the internal waves in a lake.

Despite the seemingly simplicity of Eq. 1, quantifying this relation requires high-resolution measurements of both internal and external waves, i.e., determining the pycnocline (or thermocline) and lake surface vertical offsets, respectively; proper filtering of these time series is also required. Obtaining long time series of pycnocline oscillations for the detailed analysis of internal wave frequencies and amplitudes is rather demanding in terms of equipment and time. Using conductivity, temperature, and depth (CTD) profilers during cruises provides high vertical resolution

⁴Israel Marine Data Center, Israel Oceanographic & Limnological Research, Haifa, Israel

^{*}Correspondence: nadavl@gsi.gov.il

but suffers from limited temporal resolution. Conversely, chains of sensors (e.g., thermistors) used for continuous temporal profiling measurements are usually limited in their vertical resolution over the extensive section of interest of the water column. A direct measurement for characterization of the internal waves and external waves dynamics requires a high depth and time resolution methodology, such as was applied in this study.

Dead Sea thermohaline stratification and internal waves

The Dead Sea (Fig. 1A) is a hypersaline terminal lake, located in the lowest terrestrial region on Earth, with its water level in 2012–2013 (the time of the measurements presented here) at ~427 m below mean sea level. In the past, until the 1980s, the Dead Sea was meromictic with stable stratification due to a highly diluted epilimnion. The salinity profile contributed to the stable stratification due to dilution of the surface water together with the temperature profile, and thus the water column maintained a large density difference (Hall 1981; Steinhorn 1991). Following intense anthropogenic diversion of water inflows from the Dead Sea watershed during the past four decades, the lake level has declined (Lensky et al. 2005; Fig. 1E), the surface salinity has increased, the stratification stability has weakened, and consequently the lake became holomictic in 1980 (Anati 1997; Gertman and Hecht 2002). Since then, the Dead Sea has been stably stratified throughout the 8 months of the warm season due to surface heating, i.e., stabilizing thermocline, despite a destabilizing salinity distribution driven by evaporation, i.e., destabilizing halocline (Fig. 1C,D). The stable summer stratification evolves seasonally, reaching a maximum density contrast across the pycnocline of ~2.5 kg m⁻³ during late July (Fig. 1C,D) and diminishes toward the winter due to surface cooling (Gertman and Hecht 2002; Arnon et al. 2016; Sirota et al. 2016). The temperature, salinity, and density of the upper layer are governed by atmosphere-lake interactions, salt precipitation, and double diffusion diapycnal fluxes; Arnon et al. (2016) distinguish between these governing factors, showing that in mid-summer and late summer, double diffusion plays a major role in reducing salinity from the epilimnion, whereas halite precipitation plays a major role in autumn and winter (Arnon et al. 2016; Sirota et al. 2016). Throughout the seasonal cycle, temperature plays the major role in controlling the density of the upper layer and thus on the density gradient (Fig. 1C,D). The depth of thermocline and pycnocline are identical, as the upper layer is mixed with relatively uniform temperature and salinity (Fig. 1D). Thus, the oscillations of pycnocline depth (D) can be determined by measuring high spatial resolution temperature profiles at high temporal frequency (e.g., Arnon et al. 2014a). The equation of state for the Dead Sea is

$$\rho = \rho_1 + \alpha (T - T_1) + \beta (S - S_1) \tag{2}$$

where α (-0.45 m³ kg⁻¹K⁻¹) and β (0.94 × 10⁻³ m³ kg⁻¹) are the expansion coefficients of temperature (T) and salinity

(*S*), respectively, and ρ_1 is the reference density (Anati 1997; Gertman et al. 2010).

Surface and internal seiches of the Dead Sea were investigated during the summer of 1981 by Sirkes et al. (1997). Level oscillations were measured throughout the summer, and thermocline depth oscillations were interpolated from temperature measurements of a thermistor that was located in the thermocline zone (for ~5 d in July). Despite the very limited depth resolution, the authors presented rather high correlations between the frequency analysis of the surface and the evaluated internal seiches. Additionally, their observations were limited in time, covering only a few days in mid-summer and thus could not provide an extended seasonal investigation of the internal waves in the lake. Weinstein et al. (2000) observed the internal waves in the lake for a number of days in 1994 summer within an unusual 3-yr meromictic period 1992-1995 (Stiller et al. 1984; Anati 1997; Gertman and Hecht 2002), in which the density difference between the water layers of the lake increased significantly ($\Delta \rho \geq 8 \text{ kg m}^{-3}$). This meromictic period was because of the exceptionally cool and rainy winters (1991-1992 and 1992-1993) that resulted in high discharges into the Dead Sea, a significant lake level rise (~2 m), and large dilution of the epilimnion. These exceptional winters affected the entire southeastern Mediterranean region (Halpert et al. 1993; Genin et al. 1995), most likely due to the lingering effects of the eruption of Mt. Pinatubo. We hypothesize that the trend of decreasing water column stability over the past decades, since this meromictic period, should change the amplitudes and the frequencies of the internal waves, as will be investigated within this study.

A recent study of the fine thermal stratification structure in the Dead Sea (Arnon et al. 2014a) enabled analysis of the metalimnion, using fiber optics for high-resolution temperature sensing (Selker et al. 2006; Tyler et al. 2009). Thermocline depth fluctuations of up to 15 m within a few hours were documented based on measurements having 5 min temporal and 9 cm depth resolution. High correlations between metalimnion depth fluctuations and the sea-level fluctuations were found (Arnon et al. 2014a). But, the dynamics of internal waves in the Dead Sea was not documented during the course of the seasonal stratification cycle, specifically as a response to the seasonally varying stratification stability and wind regime.

Research questions and objectives

In this study, we address the following questions regarding internal and surface waves in the Dead Sea. What is the role of the seasonal evolution of stratification stability and seasonal variations of wind intensity on the dynamics of internal waves? And, what is the role of the interannual changes in the vertical density gradient following the anthropogenic water deficit in the lake? These issues are addressed by applying a high-resolution field observation methodology of fiber optics temperature sensing together with level and wind measurements throughout the entire stratified period. Furthermore,

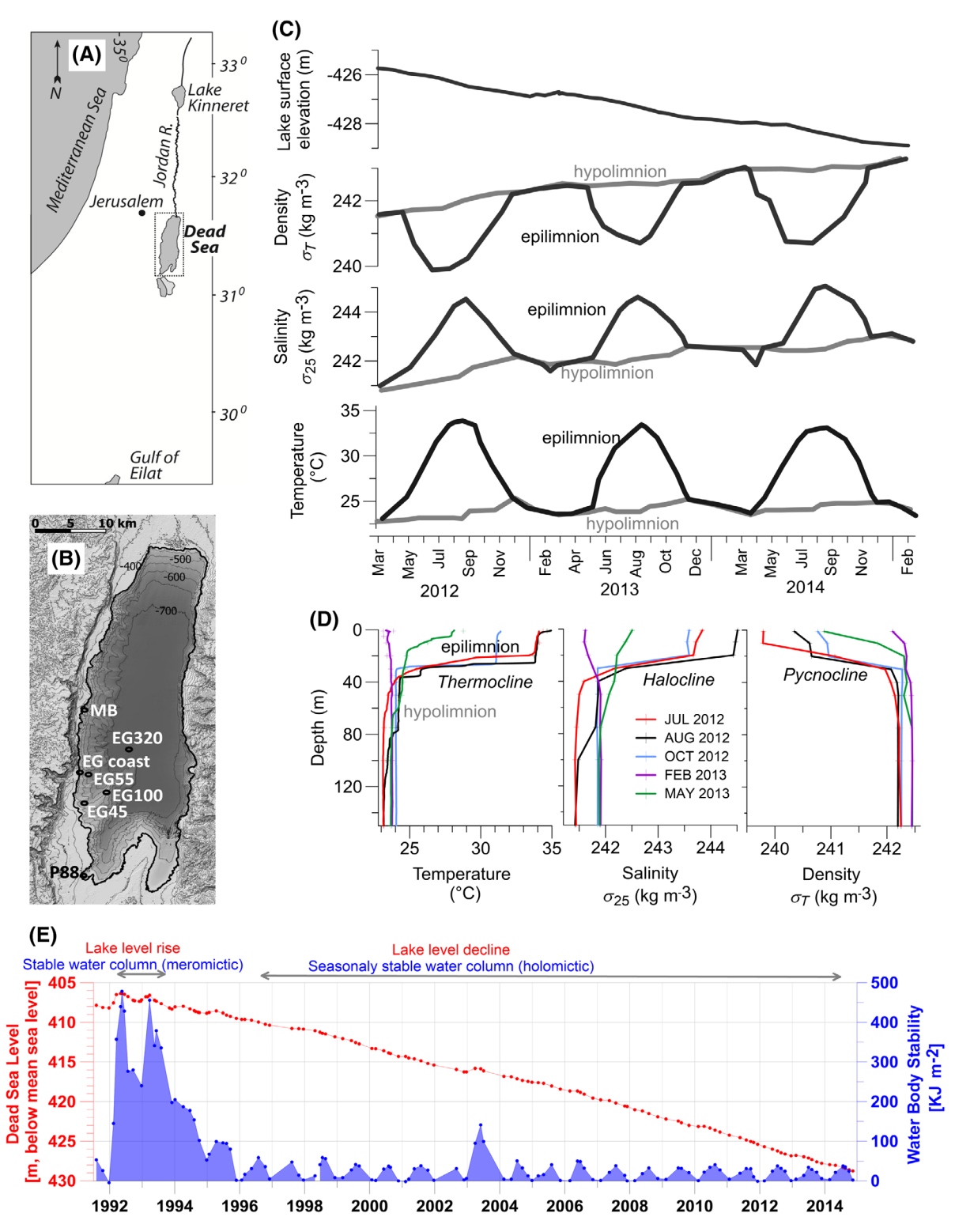


Fig. 1. (A) Location map, (B) the Dead Sea—measurement stations and bathymetry, (C) time series showing the evolution of the seasonal thermohaline layering during 2012–2014 (epilimnion—measured at 10 m; hypolimnion—measured at 50 m), (D) depth profiles at EG320 in 2012, from left to right: temperature, quasi-salinity, and density (the location of station EG320 in the panel B), and (E) time series of lake level and water-column stability (Anati 1997; Gertman and Hecht 2002) of the last two decades in the Dead Sea; note the transition from meromictic to holomictic conditions following the lake level rise, see text. [Color figure can be viewed at wileyonlinelibrary.com]

numerical model simulations of the relevant period aided the physical interpretation of the influence of seasonal stratification on the internal waves.

Methods

High-resolution temperature profiling

High spatial and temporal resolution temperature profiles were obtained using a fiber optics distributed temperature sensing (Fig. 2) system. Temperature profiles were measured using 55 m of cable (Fig. 2) with a 9 cm effective sample spacing, providing ~640 measurements along the profile. The profiles were calibrated to be accurate to $\pm 0.02^{\circ}$ C, for 5 min integration time, thus maintaining high enough frequency to observe structural changes in the water profile. The observational setup and calibration procedure were described in detail by Arnon et al. (2014a). The system recorded profiles during the stratification period, from May 2012 to January 2013.

The method of temperature sensing is based on the Raman scatter of light in optical fibers, where the ratio of the Stokes to anti-Stokes backscattered light can be used to compute the temperature at each increment of length along the fiber (e.g., Selker et al. 2006). The method was applied in lake studies, among other environmental applications (Selker et al. 2006; Tyler et al. 2009; Vercauteren et al. 2011), and is especially useful where simultaneous high temporal and vertical resolution are needed. We used a profiler with curled fiber in order to increase the depth resolution from 1 m of a straight cable to 9 cm (Arnon et al. 2014*b*).

The high-resolution data from each thermal profile were analyzed to reveal the dynamics of the thermal structure and internal waves. This was done by defining diagnostic features of the temperature profile and its first and second derivatives over depth, especially in the metalimnion. A summary of the key features in the profiles is provided in Arnon et al. (2014a).

Level measurements

Changes in the lake level were measured by a pressure sensor (Campbell CS 455 Submersible Pressure Transducer) placed near the shore on the seafloor at a depth of ~3 m. The lake level time series are the difference between the submerged pressure sensor and atmospheric pressure. Lake level time series were then detrended in order to filter out the level decline due to the negative water balance of the lake, before computing the correlations. We detrended the general lake level decline over periods of weeks, which follows a general linear trend, with ~0.3 mm d⁻¹ (depending on season). In addition, the short period (seconds) waves were filtered out by computing moving averages over 10 min.

Density and salinity measurements

Salinity was measured monthly, densitometrically (rather than with the more common method of electric conductivity, which would be out of the range of validity), and therefore, presented in quasi-salinity units—kg m $^{-3}$, i.e., the departure of the brine's density from that of distilled water at the reference temperature (Gertman and Hecht 2002; Gertman et al. 2010). Water samples were collected from representative depths (1, 10, 55, and 80 m) using Niskin bottles; the temperature was measured simultaneously using the CTD profiler (Seabird SBE19plus). The samples were kept warm to avoid salt precipitation prior to laboratory analysis. Accurate density measurements were critical for this study and were performed in the laboratory (DMA 5000) at 30°C, with an accuracy of ± 0.005 kg m $^{-3}$ (Gertman et al. 2010; Arnon et al. 2016; Sirota et al. 2016). The density difference

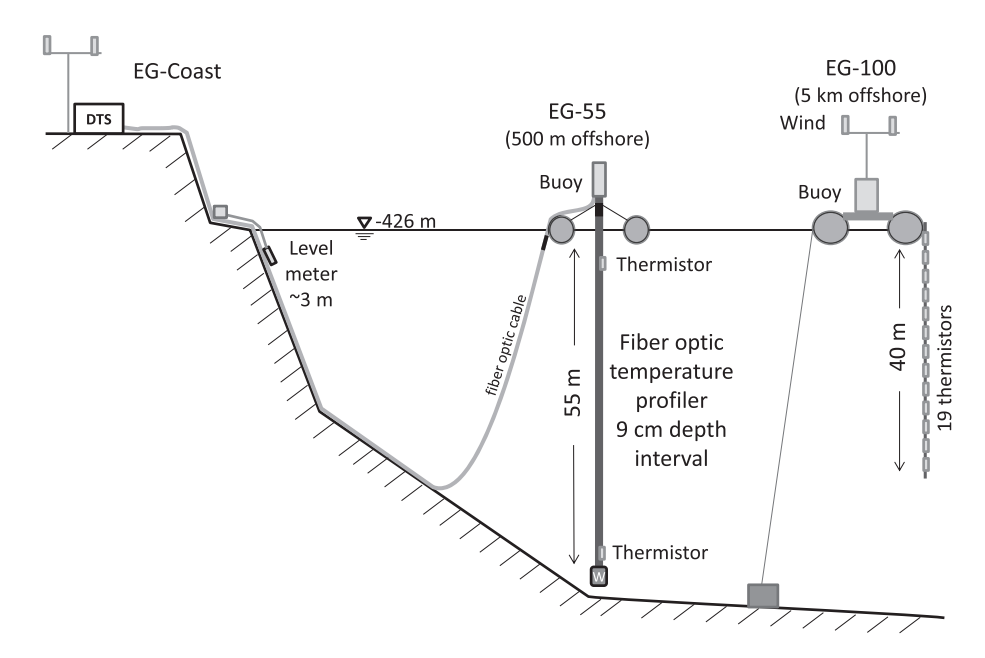


Fig. 2. Observational setup—schematic illustration of all measuring components, including water level meter, fiber optic profiler—hung from the middle of the buoy and hydrometeorological buoy. For more visual information, see Supporting Information (section S1).

between the epilimnion and hypolimnion is based on the difference of samples from 10 and 50 m. This difference is positive under holomictic conditions, as presented in this study.

Wind

Wind measurements were conducted at four stations (Fig. 1B). Aanderaa sensors were used at the offshore platform EG100 and EG coast stations (as a part of the long-term monitoring program), whereas Gill Wind Sonic sensors were used at the coastal stations MB and P88.

Model description and setup

For this study, the latest version of the Princeton Ocean Model (POM2K) was adapted to conduct the simulations. POM (Blumberg and Mellor 1987) is a three-dimensional, time dependent, free-surface, primitive equations, hydrostatic model with an embedded subgrid-scale vertical turbulence closure scheme based on the work of Mellor and Yamada (1982) with the additions described by Mellor and Blumberg (2004), and the compressibility effects neglected as the equation of state depends only on temperature and salinity as described below. The numerical scheme is based on second-order accurate finite differencing using an Arakawa-C grid, a terrain following coordinate in the vertical, and a split explicit, leap frog time scheme. Due to the unique properties of the Dead Sea water (nearly 10 times more saline than that of seawater), adaptation of the model required replacement of the standard equation of state, which is valid only for freshwater and seawater with salinities of ~40 practical salinity units (PSU; the standard oceanographic unit which is nearly equivalent to parts per thousand) or less, with an appropriate equation for the extreme salinity of the Dead Sea. The density of the Dead Sea brine is high $\sim 1.24 \times 10^3$ kg m⁻³; however, the density differences across the pycnocline are similar to common seas and lakes, <2 kg m⁻³. Presently, the code does not track the chemical composition of the Dead Sea nor significant dilutions; thus, we adopted the empirical polynomial equation of state for the solution density derived by Gertman et al. (2010) for the Dead Sea, which depends only on salinity and temperature. Ignoring chemical composition variations is justified for short-term simulations (days to weeks) that are needed for internal waves simulations. However, in longer simulations (months to years), it would be preferable to account for halite precipitation and dissolution (Arnon et al. 2016; Sirota et al. 2016, 2017) and for double diffusive fluxes (Arnon et al. 2016); both of these are beyond the scope of this article.

The model domain covers the entire northern basin of the Dead Sea with a fixed horizontal grid resolution of 200 m and 50 vertical variably spaced, sigma layers covering the entire water column from the surface to the bottom. Model layers are concentrated in the upper 40 m in order to provide good resolution of the very sharp thermocline in the stratified seasons. Twenty of the layers are located in the upper tenth of the water column so that even in the deepest point of the lake there are 20 layers between the surface and the base of the thermocline

with at least three of them in the thermocline. The bathymetry is specified based on Sade et al. (2014) (Fig. 1B) and was smoothed with eight passes of a five point Laplacian filter.

Initial conditions consisted of horizontally uniform, seasonally dependent, vertical profiles of temperature and salinity, which approximate the observations with a 25-m-deep uniform upper layer, a 5-m-thick thermocline, and a uniform layer from 30 m to the bottom. Surface forcing included temporally varying (1 h resolution), horizontally uniform wind stress. The main focus of the simulations was to study the role of wind forcing. Therefore, the model runs were limited to several weeks while heat and freshwater fluxes were neglected. The temperature, salinity, and density jumps across the thermocline, as well as the wind speed values in the various experiments, are summarized below in the Model Results—The Role of Stratification and Wind section (see Table 2 below).

Results and discussion

Seasonal characteristics of internal waves Internal waves and surface fluctuations correlation

The epilimnion was always found to be warmer than the hypolimnion during the observation period (summer 2012); the thermocline was distinct, and its vertical offsets over time represent the internal waves (Fig. 3). Furthermore, the temperature differences across the thermocline (Fig. 3) were negatively correlated with the amplitudes of the thermocline depth fluctuations (see Fig. 4), with the largest temperature contrasts and smallest thermocline fluctuations observed in August and the smallest temperature differences and largest thermocline fluctuations found in May (Table 1). Lake level and thermocline fluctuations were highly anticorrelated ($r = \sim 0.8$); the amplitude of lake level fluctuations are of ~ 1 cm, whereas the thermocline fluctuates 4–10 m, depending on the density difference (Fig. 4). Wind speed, as the primary driver for internal waves, is also presented in Fig. 4 (see more hereafter).

The effect of seasonal variations in stratification stability on the seiche amplitude

Stratification stability is expressed by the difference of densities between the layers divided by the mean density, $\frac{\Delta\rho}{\rho}$. The stability in the Dead Sea is highest during mid-summer, low during the transition seasons, and diminishes during winter (Fig. 5). The seasonal evolution of the thermocline's fluctuation amplitudes also shows a clear seasonal pattern, with minimal amplitudes during summer (~1 m) and high amplitudes in the transition period (~10 m). The amplitude of thermocline depth oscillations are based on 10 d standard deviation (moving window) of the measured thermocline depth. The observed amplitudes of thermocline offsets are in agreement with the calculated values, based on the lake level offsets and density ratio, assuming hydrostatic response (Eq. 1), as shown in Fig. 5 (blue curve and diamonds, respectively). Measured amplitude fluctuations of lake

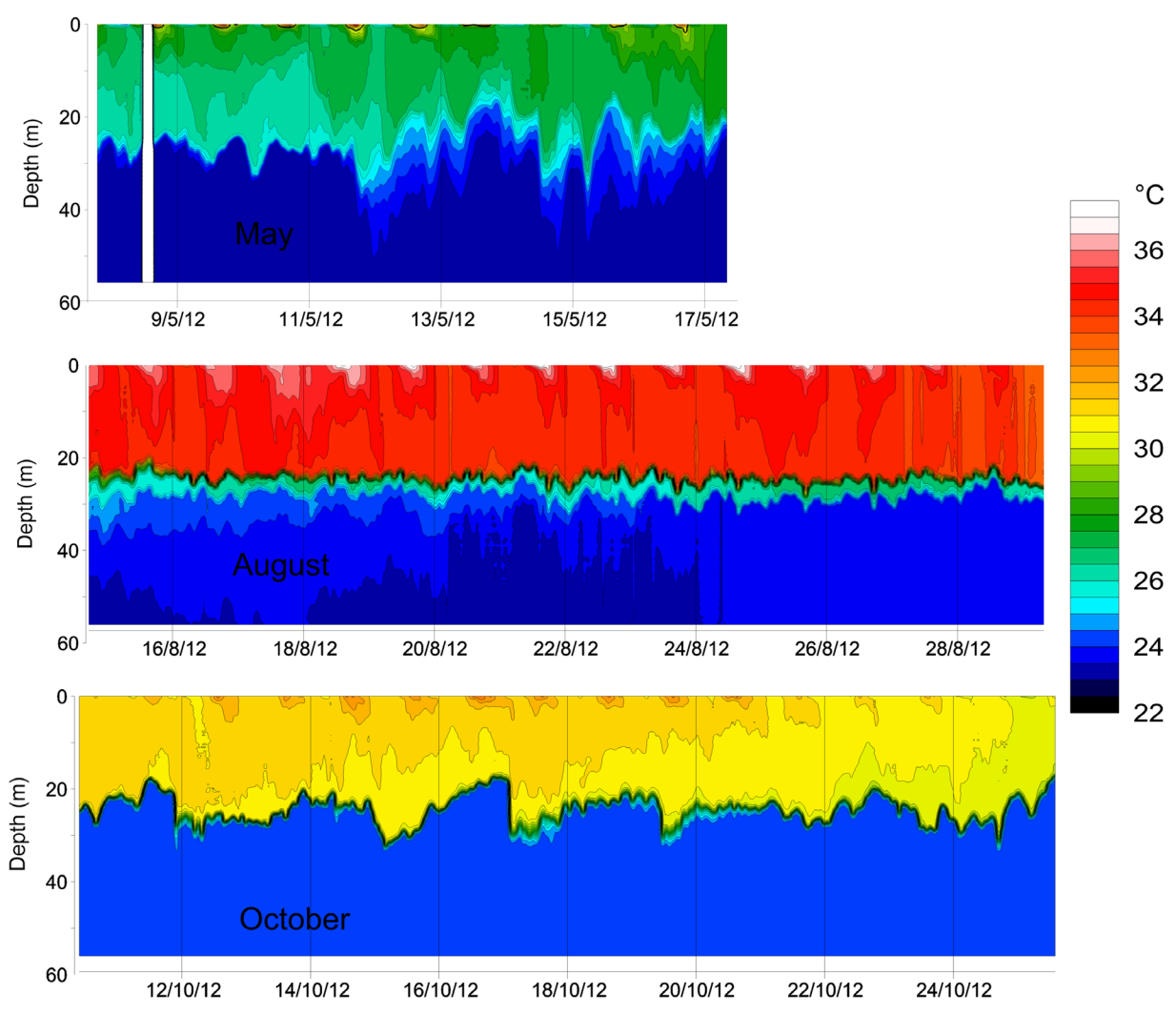


Fig. 3. Time series of temperature–depth profiles measured in May, August, and October 2012, using the fiber optic profiler at EG55 offshore station (Fig. 1B). The temperature scale is on the right (in °C). Note that in May and October, the temperature difference between epilimnion and hypolimnion is relatively small and thermocline fluctuations are large, whereas in August, the temperature difference is largest and the amplitude of the fluctuations are smallest. For more time series of temperature–depth profiles within the stratification period of 2012, see Supporting Information (section S2). [Color figure can be viewed at wileyonlinelibrary.com]

level vs. thermocline depth are presented in Supporting Information (section S3).

Hypolimnion outcropping by internal waves amplification

As the epilimnion cools during autumn, the strength of stratification diminishes, and consequently, the internal waves amplify. Figure 6 presents an event of internal wave amplification following an episode of intense wind that lasted over 2 d and caused a temporary outcropping of the hypolimnion. This event occurred at the end of the stratified season (11 November 2012), when stratification weakened significantly to $\Delta \rho \sim 0.3~{\rm kg~m^{-3}}$. The intense wind caused a strong surface level setup that was followed by a respective pressure compensation of the thermocline depth fluctuations that grew larger than the depth of the thermocline itself. This large thermocline fluctuation amplitude was

expressed as an outcropping of the hypolimnetic water to the surface on the western side of the lake.

The tendency of the lake to remain stably stratified under shear is expresses by the dimensionless Richardson number (Ri):

$$Ri = \frac{\frac{g}{\rho} \times \frac{\Delta \rho}{\Delta z}}{\left(\frac{\Delta u}{\Delta z}\right)^2} \tag{3}$$

where g is the gravitational acceleration, $\Delta \rho/\Delta z$ is the density gradient over the interface, and u is current speed. When Ri < 0.25, velocity shear can overcome a stable density stratification, and some turbulent mixing will generally occur. Indeed, during this event, the conditions favored vertical mixing, with $Ri \sim 0.15$ (density difference over the 5 m interface was ~ 0.3 kg m⁻³ and current speed difference of ~ 0.3 m s⁻¹ during an intense storm;

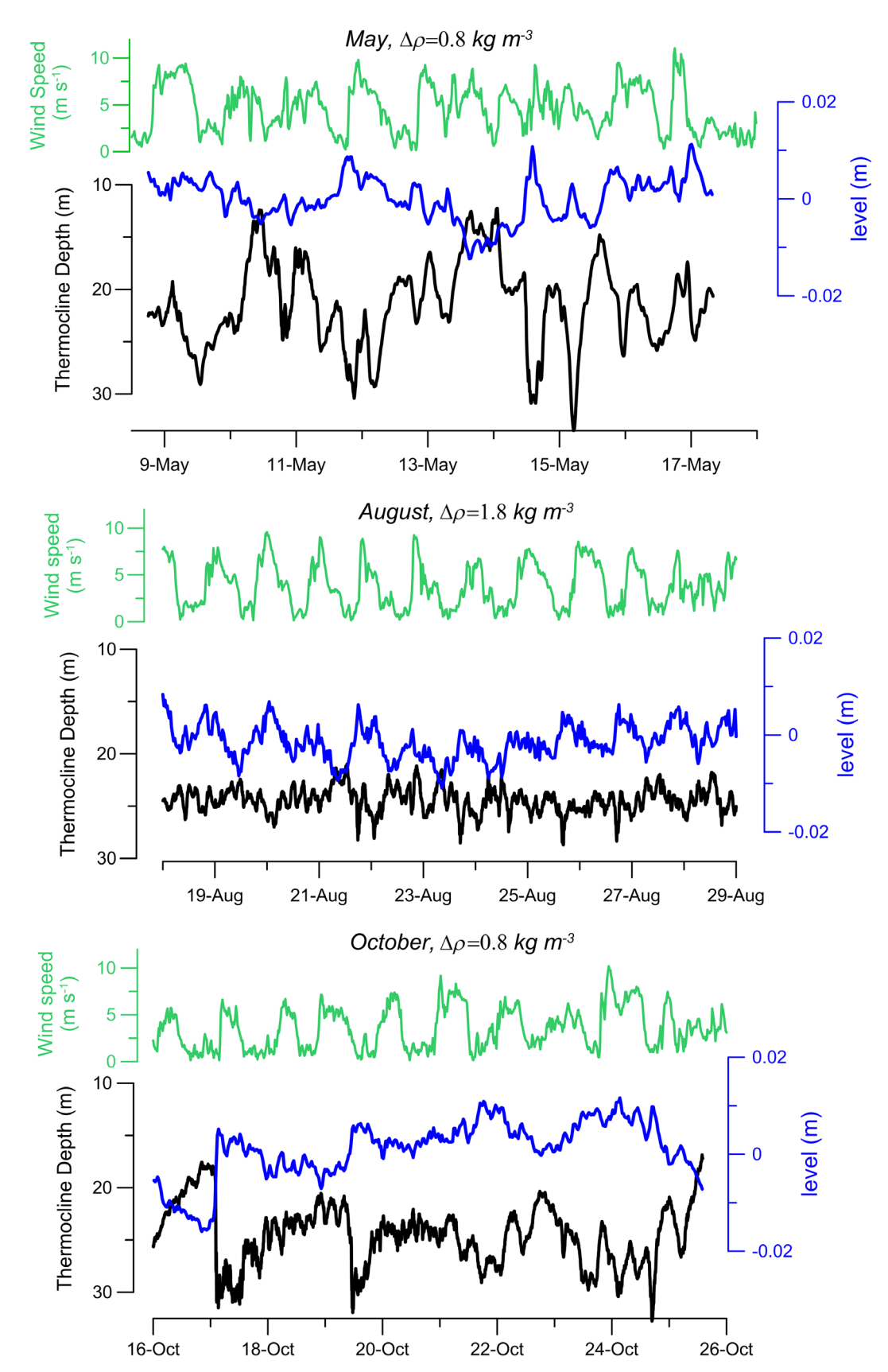


Fig. 4. Time series of wind (green) lake level fluctuations (blue) and thermocline depth fluctuations (black) during three representative periods of the stratification season: May, August, and October 2012. The correlation between thermocline depth and lake level fluctuations are high (r = 0.71, 0.82, and 0.7 for May, August, and October, respectively). Density differences between epilimnion and hypolimnion are listed at the upper part of each chart. [Color figure can be viewed at wileyonlinelibrary.com]

see Lensky et al. 2013). During mid-summer, the density stratification is larger and thus Ri is larger and the stratification is more stable, with Ri > 0.8 (density difference ~2 kg m⁻³ and a similar current value). Therefore, similar intense wind event during mid-summer would not have been expected to cause such an outcropping of the hypolimnion, and the lake would tend to remain stratified, as shown in our observations of minimal thermocline depth fluctuations (Figs. 3–5).

Power spectrum analysis of the wind and internal waves

Figure 7 shows the time series and power spectra of the observed winds, lake level, and thermocline depth during the three seasons of the stratified period. During the summer (August, middle panels), the diurnal wind cycle is the most pronounced of the seasons presented, and it is the dominant mode (period of 24 h in the power spectrum). The power spectrum also shows a secondary peak at 12 h. The summer diurnal cycle is controlled by the Mediterranean Sea Breeze (Hecht and Gertman 2003; Lensky and Dayan 2012; Lensky et al. 2018). The surface level power spectrum shows a pronounced response in the directly forced 24-h (diurnal) mode accompanied by somewhat weaker, shorter period modes at 12 and 8 h, which are also most likely related to the direct wind forcing. In the thermocline depth response, there is also a weak hint of

Table 1. Stratification parameters and internal wave amplitudes, deduced from the time series of the three periods presented in Figs. 3 and 4 (May, August, and October, 2012)

	May	August	October
$\Delta \rho$ between epilimnion and hypolimnion (kg m ⁻³)	0.8	1.8	0.8
$[\pm 0.01 \text{ kg m}^{-3}]$			
ΔT between epilimnion and hypolimnion (°C)	4	10	5
[10-d averages]			
Internal wave amplitude (m)	~10	~4	~8
[10-d averages]			

some energy at around 48 h, which is close to the first internal mode period in this season. However, this low-frequency mode does not appear to be significant. The amplitudes of thermocline depth fluctuations during summer are smaller compared to other seasons, which is consistent with the large density gradient during the summer that limits the pressure compensation of the internal waves in response to the surface waves. The response of the thermocline depth fluctuations appears at the same frequencies as those of the surface level.

In spring (May, upper panels), the wind time series is less orderly than in other seasons. The diurnal cycle is still the dominant mode, although the peak is broad and contains some energy near 36 h. There are also weaker, higher frequency peaks in the power spectrum around 13 and 9 h. The level response is more complex and variable than in summer. There appears to be a significant peak at 32 h and a broad, high-frequency peak around 12–13 h, both of which suggest a response to the wind forcing, although a direct response at the diurnal frequency is conspicuously absent. The response of the thermocline depth is similar to the fluctuations of the lake level with a broad high-frequency peak around 9–13 h and a very weak hint of a peak at 32 h, although the latter does not appear to be significant.

In autumn (October, lower panels), the wind speed time series shows a mainly diurnal cycle (24 h period), although there is a hint of some energy at lower frequencies around 72 h in the power spectrum, which is probably related to the time scale of synoptic systems in this region. There is also a weaker, high-frequency peak at 12 h. The responses of the lake level and thermocline depth fluctuation are rather complex with several episodes of very rapid increase (deepening) of the level (thermocline depth), as occurred on 17 and 20 October, followed by a gradual recovery over ~2 d. This relatively low frequency response is reminiscent of the first internal mode at this time of the year. In fact, the power spectrum analyses show most of the energy at the lower, subdiurnal frequencies with a broad peak near 72 h, which is remarkably close to the period of the first internal mode predicted by a simple two

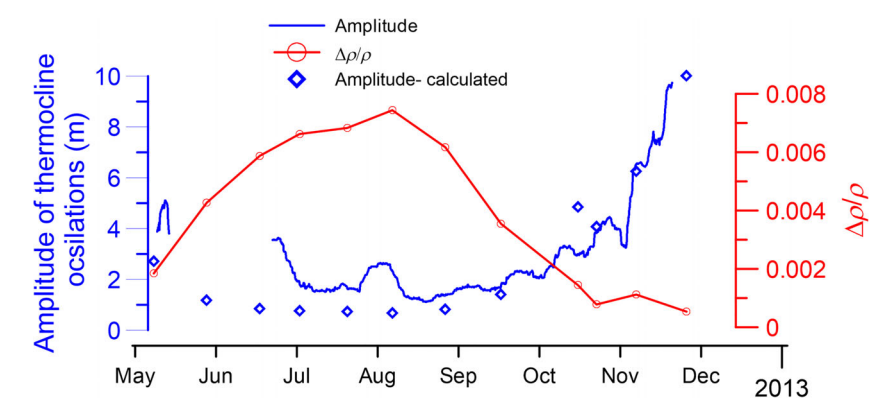


Fig. 5. The seasonal cycle of stratification stability, $^{\Delta\rho}/_{\rho}$, (red line) and the amplitude of the thermocline oscillations (blue curve). The blue diamonds are the calculated thermocline oscillation amplitude (see text). [Color figure can be viewed at wileyonlinelibrary.com]

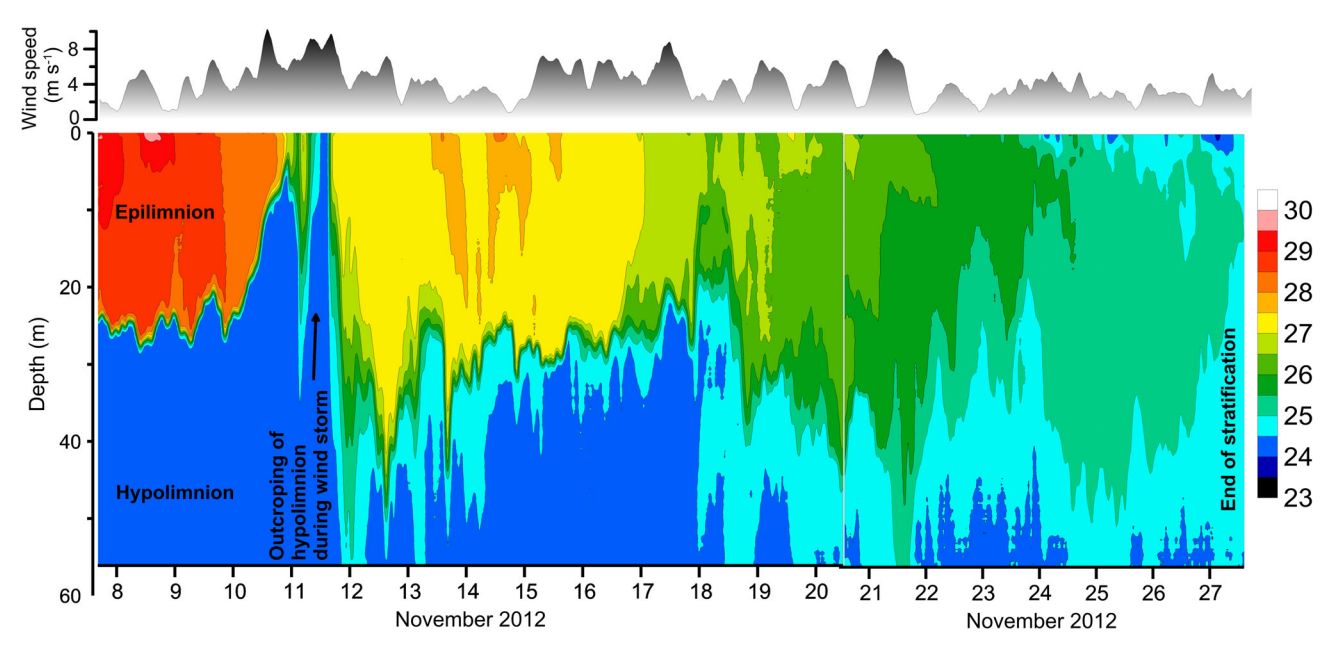


Fig. 6. Amplified internal waves resulted in a short-lived event (few hours) of rupturing of the epilimnion and outcropping of the hypolimnion (11 November 2012). Upper panel: Wind speed time series. Lower panel: Temperature–depth profile time series. Wind speed was measured at EG100 station, and the temperature profiles at EG55 offshore station (Fig. 1B). Wind speed and direction from the four stations are presented as Supporting Information (section S4). [Color figure can be viewed at wileyonlinelibrary.com]

layer model and by the normal modes simulation with the numerical model as described below. There is no peak at the 24-h mode of the diurnal cycle in contrast to the response in the summer, and there is a weaker, high-frequency peak at around 14 h. This suggests that the response of the lake at this time is close to the first internal mode, although it should be noted that this peak in the power spectrum is only marginally significant and may not be robust.

Interannual trends—The role of anthropogenic water deficit

Following the interannual trend of water diversion from the drainage basin, the salinity of the Dead Sea epilimnion increased and stratification stability decreased, and consequently, the amplitudes and periods of the internal waves changed significantly. During the brief meromictic period in 1992–1995, studied by Weinstein et al. (2000), the estimated amplitude and period of the first internal mode were ~3 m and 20 h, respectively. This is in contrast to our estimates of the holomictic conditions of the lake with much lower stratification stability and thus higher internal waves amplitude (10–20 m) and longer period of the first internal mode (~50 to 70 h). This difference can be explained by the greater density difference between the water layers of the lake due to larger diluting inflows at that time ($\Delta \rho = ~8~{\rm kg}~{\rm m}^{-3}$).

Propagation of the internal and external waves

Simultaneous measurements of the surface level and wind at four stations along the western shore of the lake (Fig. 8C) enabled observation of the surface wave's southward propagation (Fig. 8). The wind at the Dead Sea is characterized by a diurnal cycle with northerly winds at night (<8 m s⁻¹) and relatively calm daytime

winds during the warm season (Hecht and Gertman 2003; Hamdani et al. 2018; Lensky et al. 2018; Mor et al. 2018). In response to the intense northerly winds, there is a setup in the lake level at the southern end of the lake, as is seen in Fig. 8A, where the level at Sta. P88 (red curve) rose synchronously with increasing wind speed (green curve). The southward propagation of the surface wave along the western shore of the lake is indicated by the lag of the waveform, most noticeable in the maximum and minimum of the oscillations between the different stations (Fig. 8A,B). The velocity of the internal wave is estimated to be 0.48 m s⁻¹ in August and 0.43 m s⁻¹ in October (velocity is calculated as the distance between the stations divided by the time lag between the identified peaks).

Furthermore, the same analysis was applied to internal wave propagation, using temperature profiles measured at three stations (EG55, EG45, and EG100; Fig. 8C), as shown in Fig. 9. The three stations were arranged in a triangular array with legs that are 5–8 km long (Fig. 8C). The propagation of the internal wave is generally southward and is in accordance with the propagation of the surface wave. The phase speed is \sim 0.60 m s⁻¹ southward and 0.4 m s⁻¹ southeast during October. This is similar to the speed and direction of the surface waves discussed above.

Model results—The role of stratification and wind

In this section, we present results from three sets of simulations run with the model. Each set is designed to focus on a particular aspect of the internal wave dynamics as follows: (1) normal modes simulations in which the effect of the stratification strength on the leading normal mode phase speed and period is assessed; (2) idealized wind forcing in which the model is forced

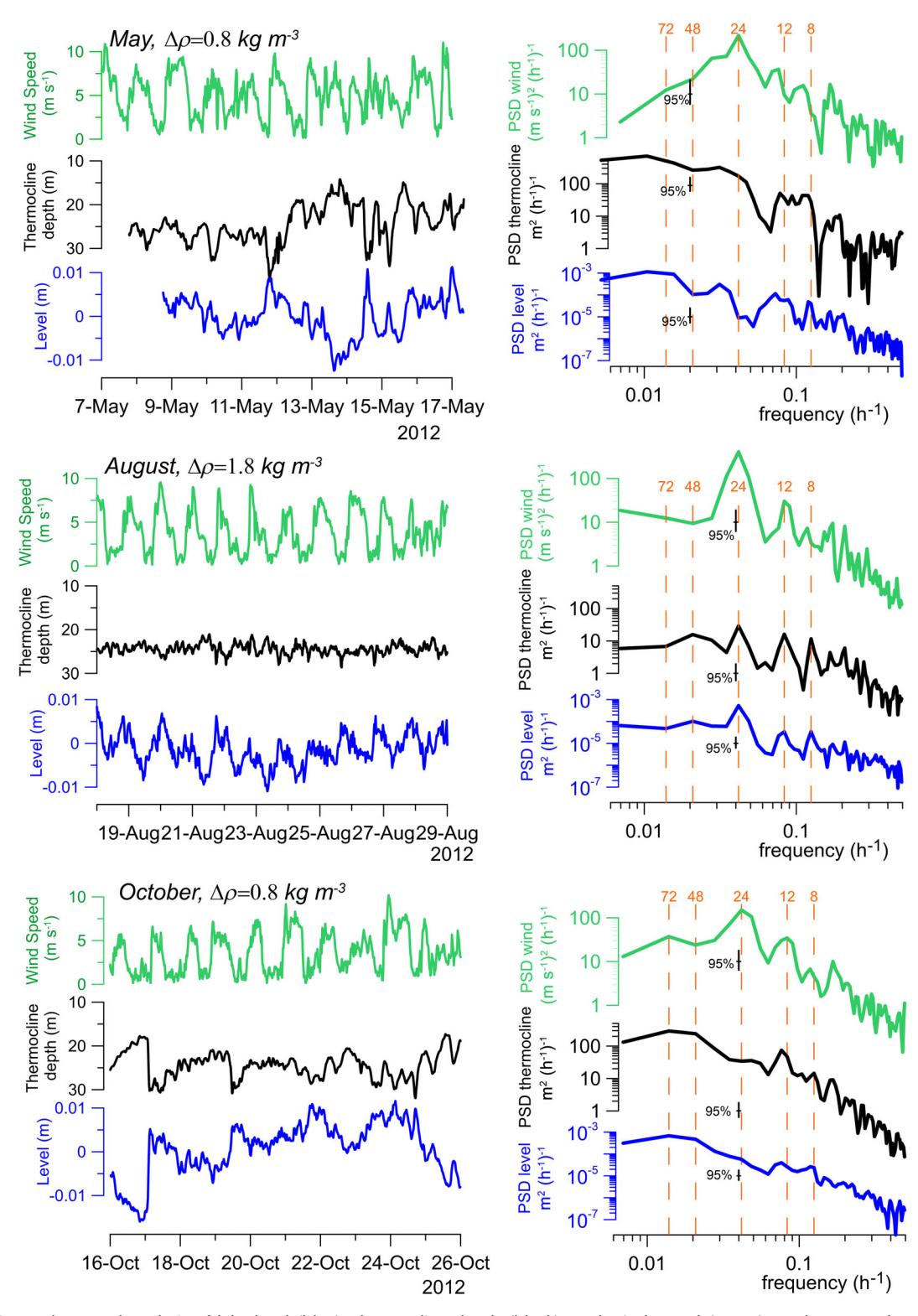


Fig. 7. Time series and spectral analysis of lake level (blue), thermocline depth (black), and wind speed (green). In the spectral analysis PSD denotes power spectral density. The vertical orange lines show representative time periods that fit the frequencies on the *x*-axis. Three representative periods are presented: May, August, and October (2012). [Color figure can be viewed at wileyonlinelibrary.com]

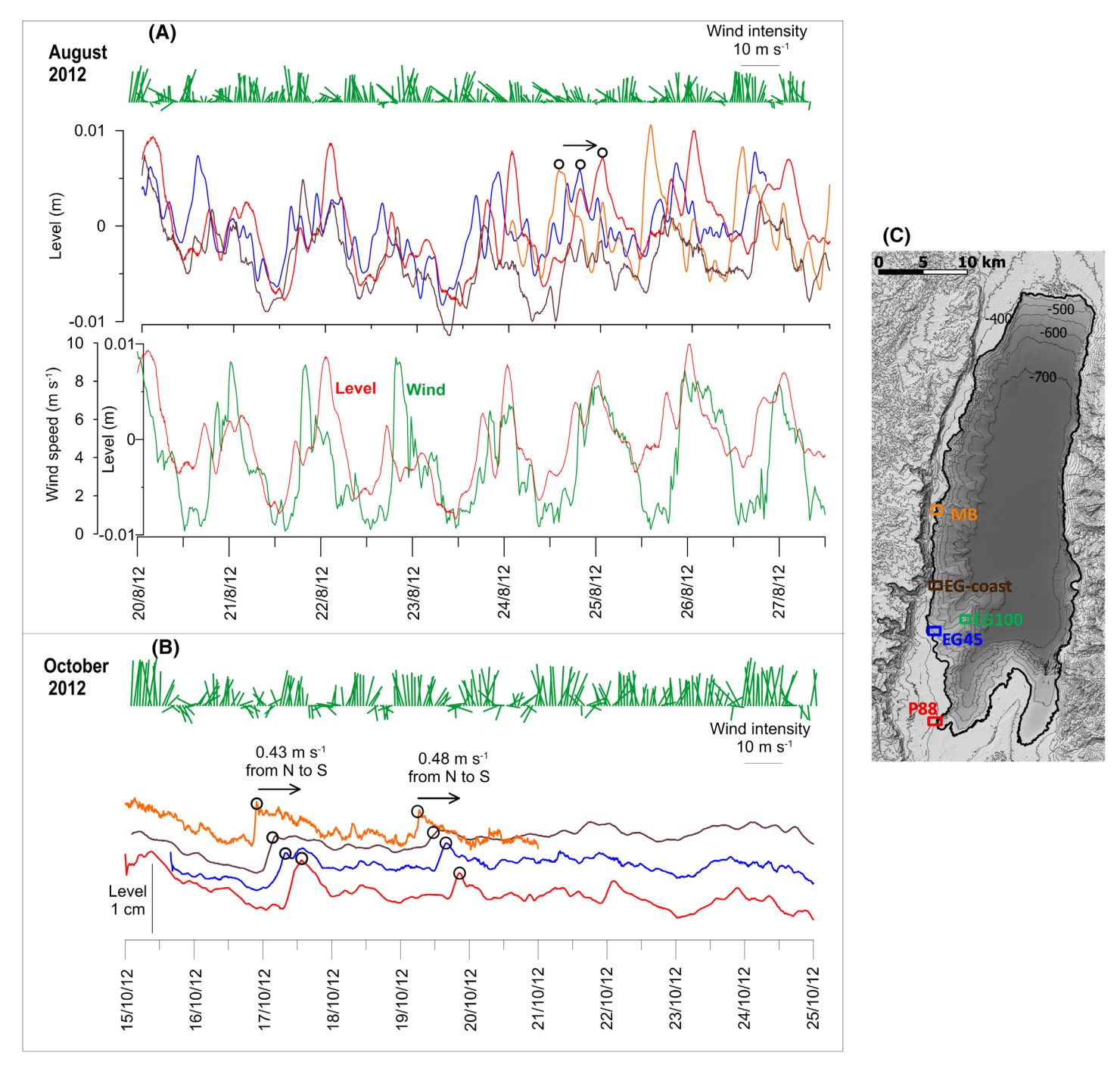


Fig. 8. Wind and level measurements along the western shore during (**A**) August (upper panel) and (**B**) October (bottom panel). Location map (**C**) of the stations is to the right. Circles are drawn at level maxima, enabling identification of the wave front and its propagation.

with a sinusoidally varying diurnal northerly wind average speeds and diurnal amplitudes; and (3) real-wind forcing. In all experiments, the initial conditions and wind forcing are horizontally uniform while the wind is time dependent. For the sinusoidally varying diurnal winds and the real winds simulations, the first 10 d are considered to be the spin-up period and the analysis focuses on the subsequent 10–15 d. In the normal modes simulation, a constant wind blows for the first 24 h and is then abruptly

turned off. Details of the initial conditions (stratification) and the surface forcing for all of the simulations are summarized in Table 2.

Normal modes analysis

As the equilibrium of the surface of an enclosed or semienclosed body of water (i.e., lake) is disturbed by an impulsive force, the surface level will begin to oscillate in response to the restoring force of gravity as the system attempts to return to equilibrium.

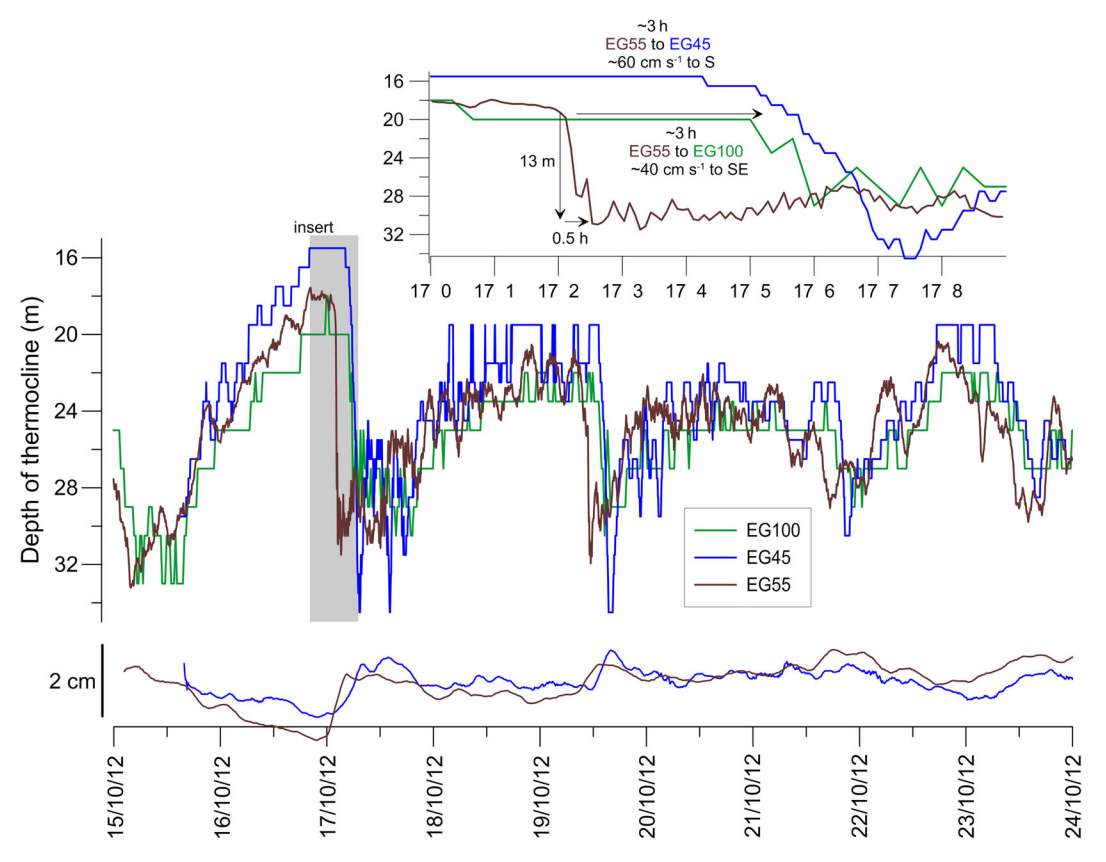


Fig. 9. Time series of thermocline depth (upper panels) and lake level (lower panel), measured at three stations (see locations in Fig. 8C). The upper panel is an insert of the shaded bar. The propagation of the internal and external waves is indicated. Current measurements from this period are presented in Supporting Information (section S5).

In a stratified fluid, the pycnocline is also expected to oscillate in response to the hydrostatic pressure changes caused by the surface slope. The surface level and thermocline fluctuations are expected to be out of phase as demonstrated above by the measurements. These oscillations will occur at particular characteristic frequencies or periods, which are determined by the size and shape of the basin, the water depth, and the stratification. The two modes of oscillation will be the rapid external or barotropic mode and the slower internal or baroclinic modes. The external mode has phase speed $C_{\rm ext} = (gH)^{1/2}$, where $g = 9.81~{\rm m~s^{-2}}$ is the acceleration of gravity and H is the total water depth in meters. For $H = 205~{\rm m}$ (average depth of the Dead Sea),

Table 2. Initial conditions (stratification) and wind forcing for all simulations. All initial conditions and winds are horizontally uniform, whereas the wind forcing varies in time

	Initial conditions $T_{\text{hypolimnion}} = 24^{\circ}\text{C}$, $S_{\text{hypolimnion}} = 278 \text{ PSU}$			
Experiment	ΔT (°)	ΔS (PSU)	Δho (kg m ⁻³)	Wind forcing
Normal modes—Oct	6	2	0.8	Northerly 10 m s ⁻¹ for 24 h
Normal modes—Aug	10	2.95	1.8	Northerly 10 m s ⁻¹ for 24 h
Normal modes—meromicitic	9	-6	7.8	Northerly 10 m s ⁻¹ for 24 h
Sinusoidal wind—1	6	2	0.8	Northerly, average 6 m s ⁻¹ , diurnal amplitude 2 m s ⁻¹
Sinusoidal wind—2	6	2	0.8	Northerly, average 6 m s ⁻¹ , diurnal amplitude 4 m s ⁻¹
Sinusoidal wind—3	6	2	0.8	Northerly, average 6 m s ⁻¹ , diurnal amplitude 6 m s ⁻¹
Sinusoidal wind—4	6	2	0.8	Northerly, average 2 m s ⁻¹ , diurnal amplitude 2 m s ⁻¹
Sinusoidal wind—5	6	2	0.8	Northerly, average 4 m s ⁻¹ , diurnal amplitude 2 m s ⁻¹
Sinusoidal wind—6 (same as sinusoidal wind—1)	6	2	0.8	Northerly, average 6 m s ⁻¹ , diurnal amplitude 2 m s ⁻¹
Real wind—Oct	6	2	0.8	Real winds from buoy, 5–29 Oct 2012

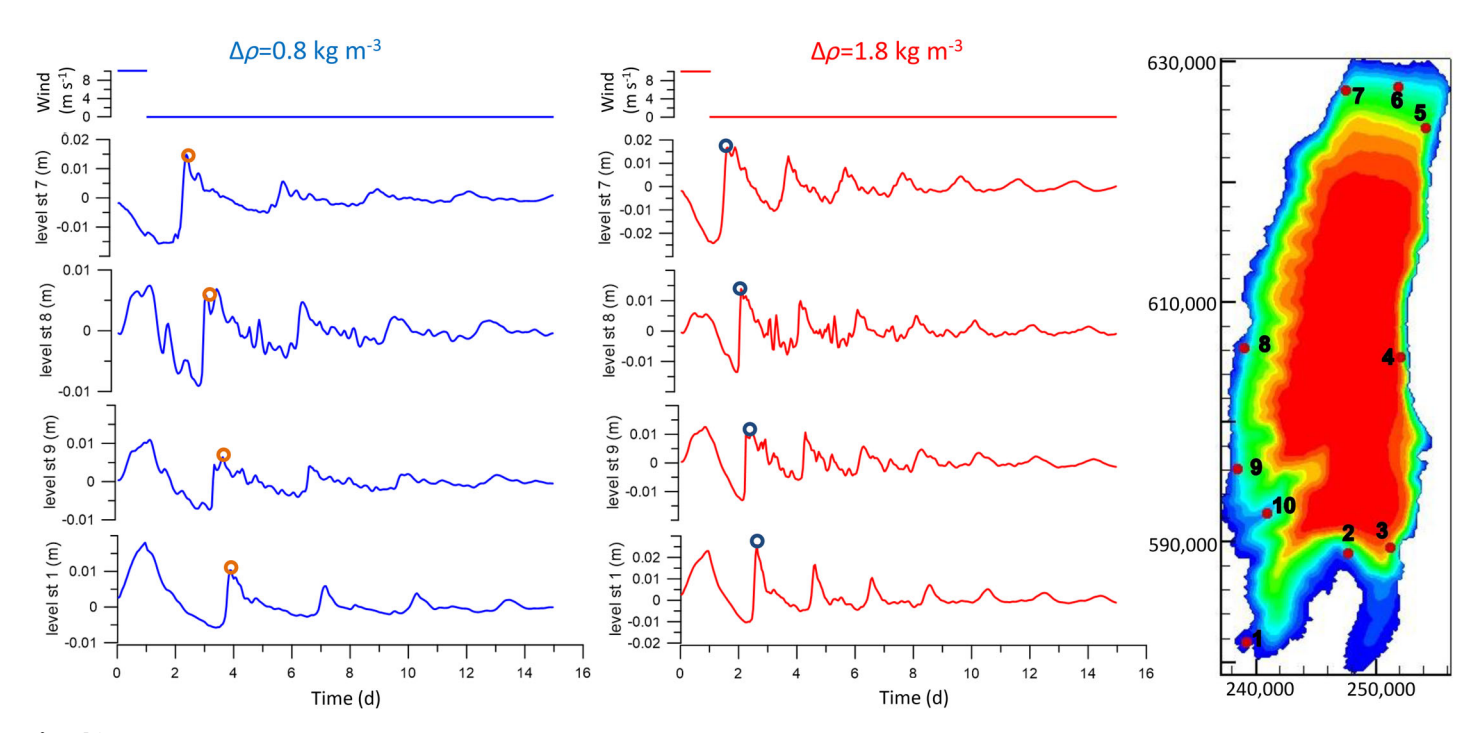


Fig. 10. Simulated time series of the wind and surface level at four stations along the west coast of the Dead Sea for the normal modes simulations in October (blue) and August (red). A location map of the stations is shown on the right. The circles indicate the wave front timing (visually identified) at the different stations showing the propagation of the wave from north to south. [Color figure can be viewed at wileyonlinelibrary.com]

 $C_{\rm ext}$ = 44.8 m s⁻¹. For a length of 47 km, the external wave period is on the order of ½ h. The amplitude of the external wave will most likely be less than the amplitude of the wind setup, which for a northerly wind of 8 m s⁻¹ blowing over the Dead Sea will be less than 0.003 m as estimated from the steady state, one-dimensional wind setup in which the surface slope balances the wind stress. Thus, we do not expect this mode to contribute significantly to the surface level signal. For a continuously stratified fluid, there can be an infinite number of baroclinic modes (expressed as velocity direction reversals in the water column), although the amplitudes of the first few modes are usually the largest. In fact, in many cases, the first baroclinic mode, associated with a two layer fluid, is the dominant mode (e.g., Horn et al. 1986). The phase speed of this mode is given by $C_{\text{int}} = \sqrt{\frac{g(\rho_2 - \rho_1)h_1h_2}{\rho_2(h_1 + h_2)}}$ (Watson 1904), where ρ is the density, h is the layer thickness, and the subscripts 1 and 2 refer to the upper and lower layers, respectively (Wedderburn 1912). Based on the typical profiles shown in Fig. 1, we can estimate $h_1 = 25$ m, $h_2 = 180$ m, and $\rho_2 = 1242$ kg m⁻³. The density difference, $\rho_2 - \rho_1$, is approximately 0.8 kg m^{-3} in October and 1.8 kg m⁻³ in August, and therefore, the first internal mode phase speeds will be 0.37 and 0.56 m s⁻¹, respectively. Assuming the length of the lake to be L = 47 km, the periods of the internal wave, $2L/C_{int}$, are estimated to be 70.6 h in October and 46.7 h in August. We note that in the spectral analysis of the observed thermocline depth (Fig. 7), there is a hint of some energy at 48 h in August, even though it is marginally significant, whereas in October, the 72 h mode contains most of the energy.

In order to compute the dominant normal modes of the lake, we ran two simulations using the model in which a constant northerly wind of 10 m s⁻¹ blows for 24 h and was suddenly turned off. The two simulations differ only by the density difference across the pycnocline, referring to the October and August observations (0.8 and 1.8 kg m⁻³, respectively). The relaxation of the surface setup and the pycnocline set-down are then followed for an additional 14 d. By following the wave front, the north to south propagation of the wave is evident (Fig. 10). The front propagation is visually identified in the extrema of the oscillations as indicated by the circles on the time series. The wave front moves from Sta. 7 to Sta. 1 (47 km) in ~24 h in August and ~36 h in October, corresponding to a speed of 0.5 and 0.36 m s⁻¹, respectively. The left panel in Fig. 11 shows the time series of the simulated surface level and the pycnocline depth (defined by the depth of the isotherm half way between the upper and lower layers) at a grid point near EG100. In both figures, it is quite clear that the internal waves on the thermocline are out of phase with the surface oscillations and that the ratio between the amplitude of the surface to thermocline oscillations is on the order of 0.001, as expected.

Spectral analyses of the surface and thermocline depth normal modes suggest that subdiurnal, low-frequency oscillations associated with the seasonally varying first baroclinic mode are the dominant modes (Fig. 11). In October, the spectral peak appears near 74 h, whereas in August, it is near 45 h. Both of these values are remarkably close to the values estimated from the simple two-layer calculation using the average depth of the lake (70.6 and 46.7 h), although some caution is necessary regarding the October peak as

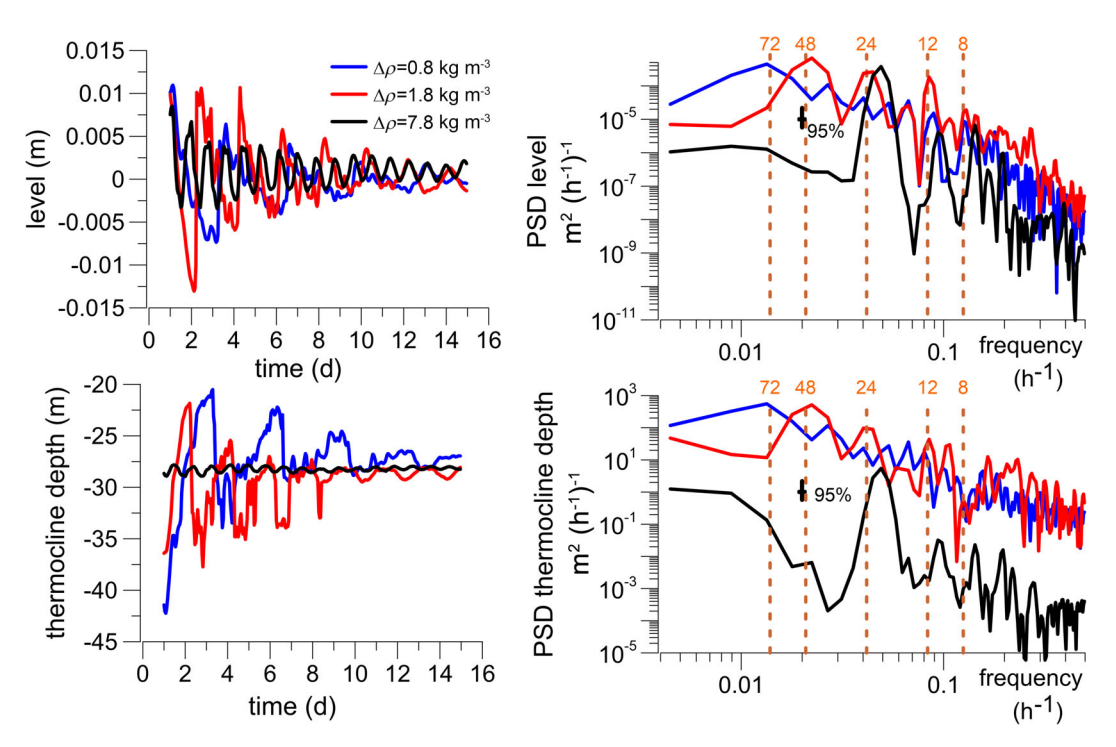


Fig. 11. Time series (left panels) of the surface level (upper) and pycnocline depth (lower) for the normal modes simulations in August ($\Delta \rho = 1.8 \text{ kg m}^{-3}$, red lines) and in October ($\Delta \rho = 0.8 \text{ kg m}^{-3}$, blue lines); meromictic conditions are also shown ($\Delta \rho = 7.8 \text{ kg m}^{-3}$, black lines). Spectral analysis (right panels) of the surface level (upper) and pycnocline depth fluctuations (lower) in August and October and for meromictic conditions (red, blue, and black, accordingly). [Color figure can be viewed at wileyonlinelibrary.com]

it is the range of low resolution in the spectrum. Furthermore, the propagation velocity of the dominant first mode as evaluated from the measurements of the level and thermocline depths at several locations are also in the same range, with periods of ~70 and ~50 h during October and August, respectively, although we must recall that the measured data are also influenced by the wind frequency and intensity, in contrast to the normal modes simulation. For the historical "meromictic conditions," the density difference between the water layers was chosen to be 7.8 kg m⁻³ to fit the conditions of the Dead Sea within the meromictic period of 1992-1995 presented in Weinstein et al. (2000). With such a large density difference, there is no low frequency response and the main mode of the level fluctuations has a period of at ~20 h. The thermocline's response is weak at the ~20-h period as expected from the two layer model (Eq. 1) with a large density difference. Consequently the anthropogenic lake level drop of the Dead Sea, followed by a stability change of the stratified water column, has led to a significant shift of the natural frequencies of the lake toward lower values (i.e., longer periods).

Upon examining the power spectra of the observed level and thermocline depth oscillations (Fig. 7) in view of the normal modes model analysis, we see that during October while the diurnal mode in the wind is dominant, the power in the lower frequency (~72 h) mode is 24% of the power of the diurnal mode. And yet, the response of the thermocline depth is most energetic at that lower frequency mode (very close to the first internal mode), whereas it is nearly absent in the diurnal mode. In

contrast, during August, the power in the respective low-frequency mode of the wind is only 3% of the power of diurnal mode, and the lake response is mainly diurnal. This difference suggest that the leading natural frequency of the lake may be excited only when a substantial amount of the wind forcing is imparted close to that frequency, possibly due to resonance. Conversely, when the wind forcing is concentrated around a particular frequency (e.g., diurnal) which is far from the leading natural frequency, as in August, the lake response will appear mainly as a directly forced response to the wind (Rozas et al. 2014).

The wind effect on internal waves

Wind is the primary momentum source for the waterbody dynamics, inducing surface currents and basin-scale internal waves. After exploring the natural frequencies of the Dead Sea in peak stratification and in marginal stability conditions (previous section), we wish to explore the role of wind speed and frequency on the frequencies and magnitudes of the surface and internal waves.

To test the response of the internal waves to different wind speeds at the diurnal frequency, we ran the model with a repeating sinusoidal diurnal wind for transition season (October) stratification of $\Delta \rho = 0.8$ kg m⁻³. Two set of experiments were run—one in which the average wind speed was kept fixed at 6 m s⁻¹ but the amplitude of the diurnal cycle was 2, 4, or 6 m s⁻¹ and a second set in which the diurnal amplitude was fixed at 2 m s⁻¹ but the average wind speed was 2, 4, or 6 m s⁻¹. The results after a spin-up

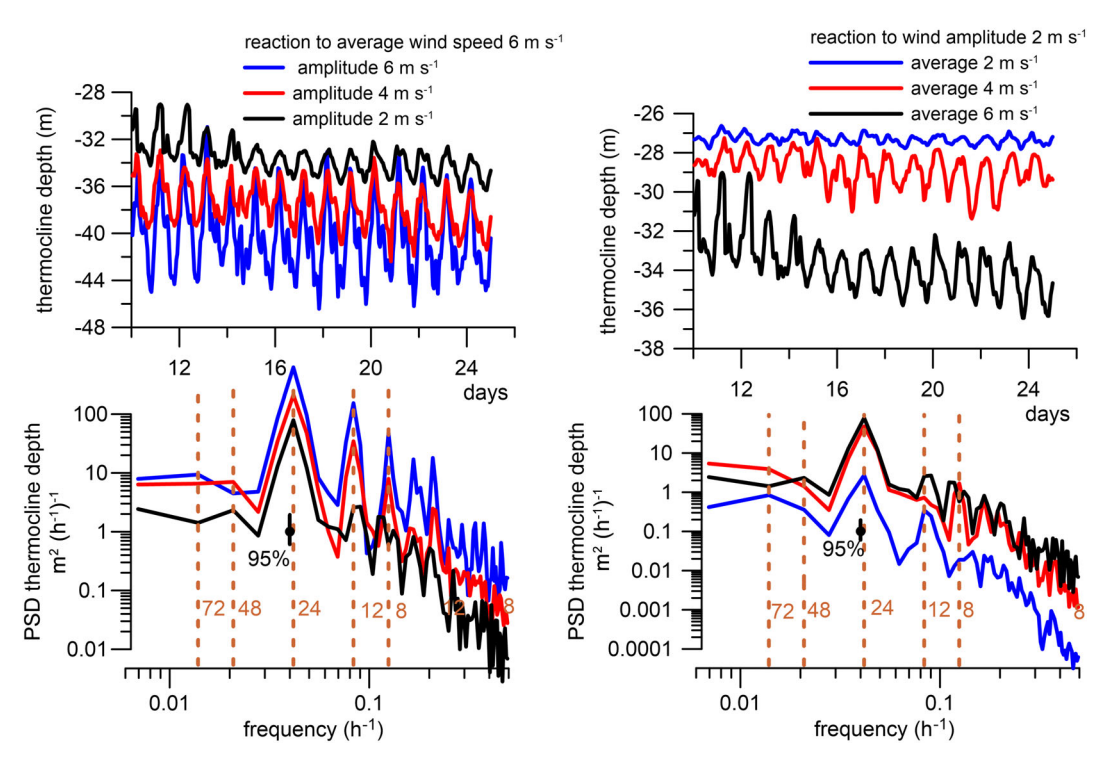


Fig. 12. Simulated thermocline depth (upper panels) and the power spectra (lower panels) for synthetic sinusoidal diurnal wind forcing experiments: average wind speed of 6 m s⁻¹ and diurnal amplitudes of 2, 4, and 6 m s⁻¹ (left panels) and average wind speed of 2, 4, and 6 m s⁻¹ with diurnal amplitude of 2 m s⁻¹ (right panel). Quality testing of the model runs is presented in Supporting Information (section S6). [Color figure can be viewed at wileyonlinelibrary.com]

period of 10 d are shown in Fig. 12, where the fixed average wind cases are in the left panels and the fixed diurnal amplitude cases are in the right panels. From both time series, it is clear that as the wind speed increases, more kinetic energy is imparted into the lake as expressed by a deepening of the average depth of the thermocline. For the fixed average wind speed simulations (left panels), increasing the amplitude of the diurnal cycle causes a deepening of the thermocline as well as a noticeable corresponding increase in the amplitude of the thermocline depth fluctuations. For the fixed diurnal amplitude simulations (right panels), the thermocline depth increases in accordance with the increase in the average wind speed in addition to a small increase in the thermocline depth fluctuation. In the power spectra of both sets of experiments, it is clear that the dominant mode of response of the thermocline depth fluctuations is at the diurnal wind forcing frequency. As expected, an increase in the wind magnitude leads to an increase in the power of the diurnal mode response. Several higher frequency modes are also excited, most noticeably at 0.0833 and 0.125 h^{-1} (12 and 8 h, respectively). However, these higher frequency modes appear to be significant only in the highest wind speed simulations. For the Sinusoidal Wind—3 experiment (strongest winds considered), the power of the 12 and 8 h modes are 25% and 8%, respectively, of the diurnal power.

Simulations using observed wind forcing

In this section, we present the results from a 25-d simulation forced with the observed October winds (from the EG100

offshore station) and a density contrast of $0.8~kg~m^{-3}$. As noted above, the model is initialized with horizontally uniform temperature and salinity profiles. We also use temporally varying but horizontally uniform wind forcing, which may impose some limitations on the comparison between the observed and model results. The implications of this will be discussed below. The first 10~d of the simulation are considered to be the spin-up period and are not included in the analysis.

The time series of the observed wind as well as the simulated and measured surface level and thermocline depth oscillations are shown in Fig. 13 for the period 16–26 October 2012 (left panels) together with the corresponding power spectra (right panels). As discussed above, in the power spectrum of the wind (upper right panel), a clear dominant peak appears at 24 h in addition to a hint of some lower frequency energy at around 72 h and a weaker, high-frequency peak around 12 h.

In the observed surface and thermocline oscillations (blue lines), two events of gradual surface decline (thermocline rise) over approximately 2 d followed by a rapid rise (decline) over a few hours can be seen during the first week. A weaker event also appears between days 8 and 11. This is expressed in the power spectra by low-frequency (subdiurnal) energy with a peak at 72 h, although as discussed above (*see* Fig. 7), this peak is marginally significant and may not be robust. No obvious peak near 24 h appears, although there are two weaker peaks around 13 and 8 h. The model (pink lines) reproduces this episodic variability, although the events on day 4, day 7, and day 9 are delayed by nearly 1 d. We also note that

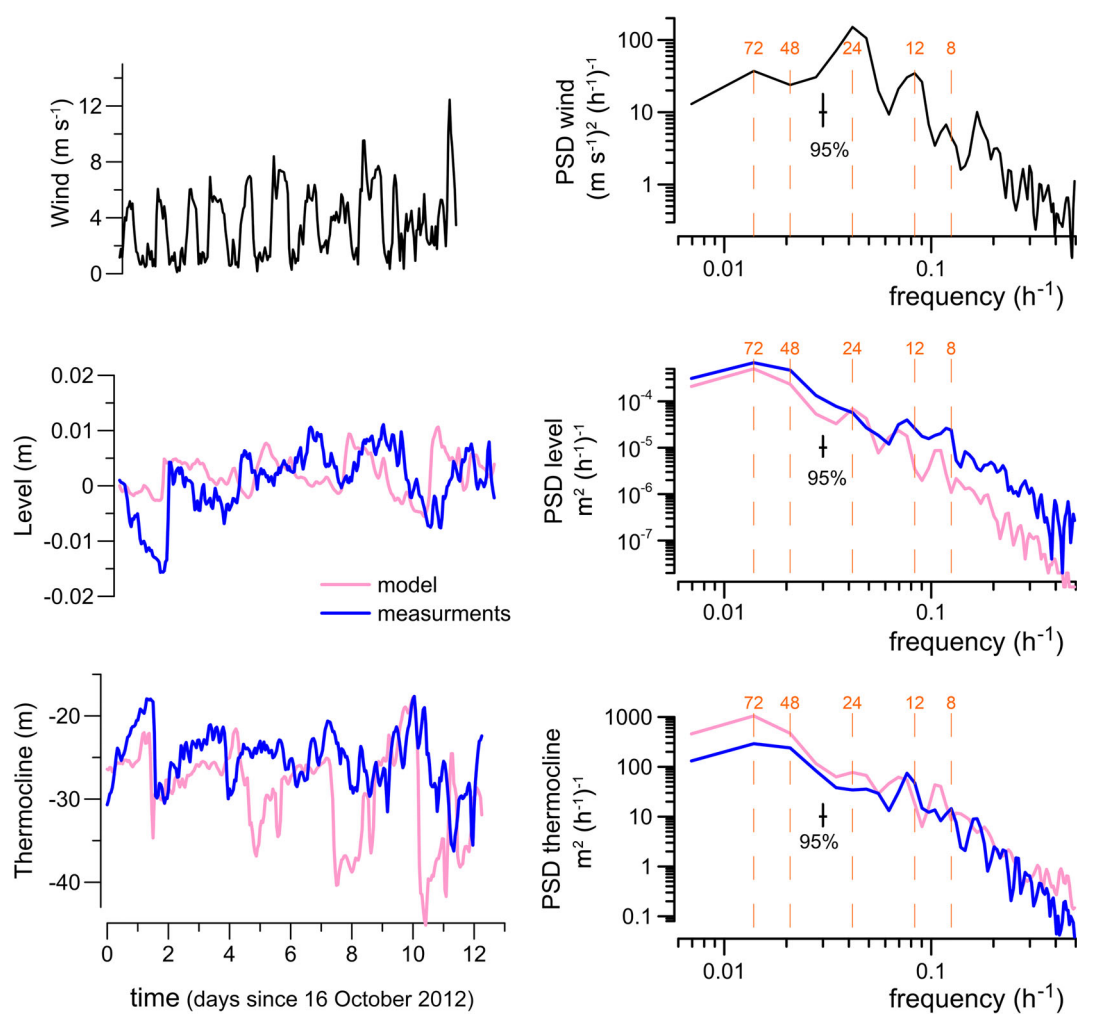


Fig. 13. Time series and power spectra of observed wind speed (upper panels) and simulated (pink) and measured (blue) surface (middle panel) and thermocline oscillations (lower panel) using wind forcing from October 2012. [Color figure can be viewed at wileyonlinelibrary.com]

the simulated amplitude of the thermocline fluctuations in the later part of the period shown is larger than the observed fluctuations. This explains the higher values of low-frequency energy in the simulated power spectrum as compared to the observed. Nevertheless, the model properly reproduces the peak at 72 h. The other mode that is noticeable in the observed spectra appears near 14 h. The model also successfully reproduced this mode. In addition to the more energetic low-frequency peak in the model, the main difference between the simulated and observed spectra is that the model produces a weak 24 h mode, which is not apparent in the observations. We note that this simulated diurnal mode appears somewhat exaggerated due to the use of a logarithmic scale. In fact, the power of this diurnal mode is only 7% of the low-frequency mode, whereas in the observed spectrum, the power of the diurnal mode is 16% of the low-frequency mode. This is possibly linked to the assumption of spatially uniform winds, which appears to be adequate for forcing similar simulations in small lakes (e.g., Forcat et al. 2011), but for larger lakes such as the Dead Sea, the wind stress curl may be a significant source of vorticity and therefore affect the spectral characteristics of the circulation in general and internal waves in particular (e.g., Schwab and Beletsky 2003). Simulations with a high-resolution, regional atmospheric model for this area (S. Brenner pers. comm.) suggest that there may be significant spatial variability of the wind, especially across the lake (west to east), which could lead to a significant wind stress curl. This point warrants additional investigation, which is beyond the scope of this study. Similarly, the underlying mechanism which excites lower, subdiurnal frequency internal waves close to the first internal mode should also be further investigated. One possibility is that the weak subdiurnal signal in the wind, which is close to the frequency of the first internal mode, forces a resonant response at the natural frequency of the lake as suggested by Rozas et al. (2014). This is further suggested by the fact that the power in the low-frequency mode in the wind is 24% of the power in the diurnal mode.

Looking at the spatial progression of the simulated internal waves, a counterclockwise rotation of the internal waves around the lake can clearly be seen (Fig. 14). This is consistent with the observed propagation of the internal waves along the

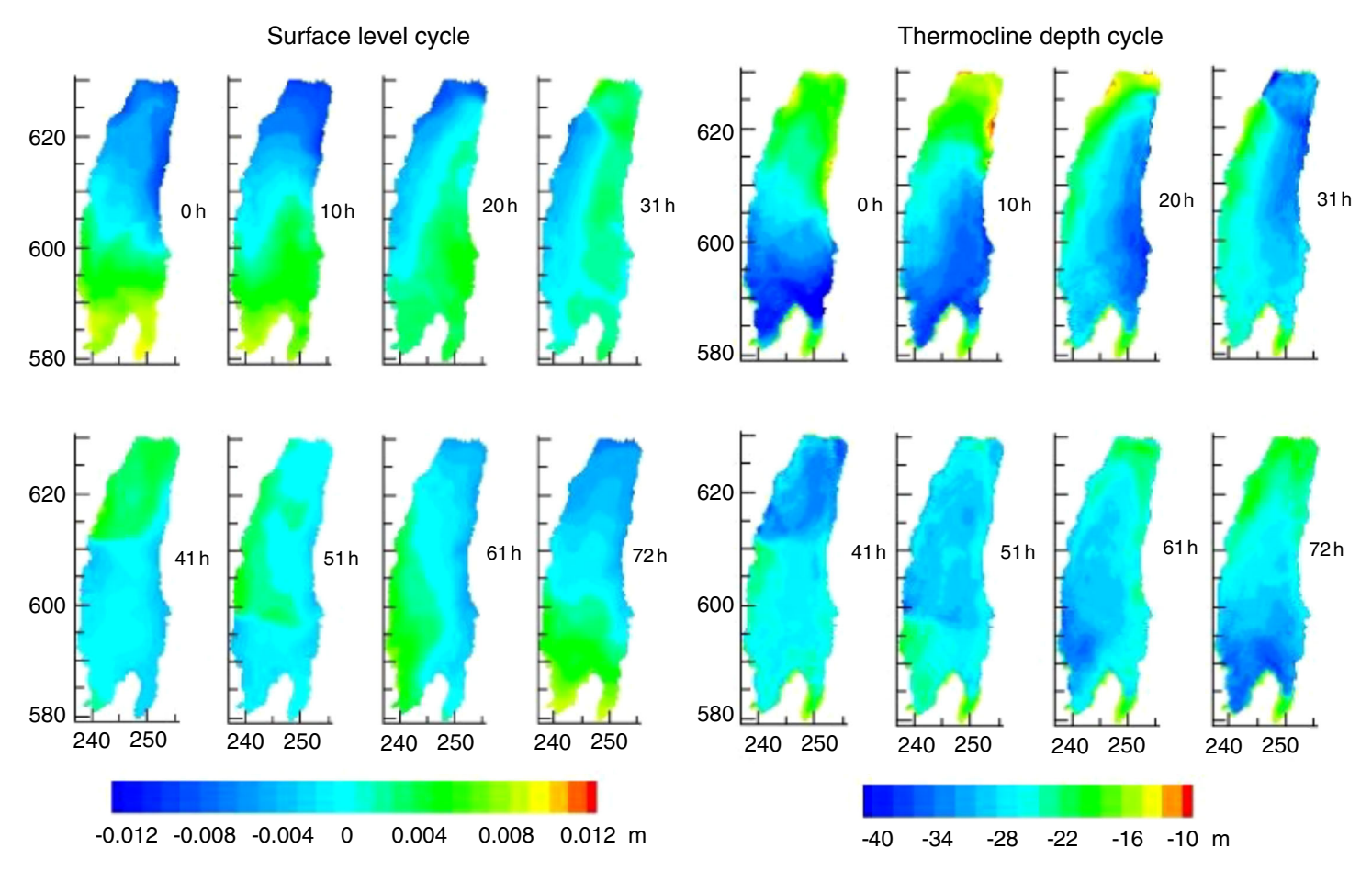


Fig. 14. Spatial progression of the internal waves in the surface height (left) and in the depth of the thermocline (right) for the 3-d model period 16 October 2012, 00:00 h, to 19 October 2012, 00:00 h. The time in hours from 16 October 00:00 h is noted on each panel.

western side of the lake from north to south as shown above in Figs. 8 and 9. The surface level and thermocline depth are out of phase as expected.

One final factor that we consider is the influence of the earth's rotation on the internal waves in the Dead Sea. Rotational effects on internal waves are generally expected to occur in large lakes, but they appear to be ubiquitous and have even been observed in small lakes (e.g., Forcat et al. 2011) as well as in medium-size long, narrow, and deep lakes (e.g., Horn et al. 1986). The importance of rotational effects on the internal waves is assessed by the value of the Burger number, Bu = c/fL, where, c is the internal wave phase speed, f is the Coriolis parameter, and L is the length scale (width of the lake). As the internal Rossby radius of deformation is defined as Ro = c/f, Bu is the ratio between the Rossby radius and the length scale of the lake. When Bu is less than unity, the earth's rotation is expected to be important. Taking L = 15 km and a typical October first-mode internal wave phase speed $c = 0.37 \text{ m s}^{-1}$, we find the Burger number is ~0.33, and thus, rotational effects are expected to be important. In this case, Ro ~ 5 km is a measure of the trapping distance of the Kelvin waves, which is consistent with the results shown in Fig. 14. In order to confirm the importance of the rotational effects on the internal waves in the Dead Sea, we reran the October simulation with no Coriolis force. When the Coriolis force is not considered, the circulation consists mainly of a north-south sloshing along the long axis that is fairly uniform across the lake.

Summary and conclusions

In this work, we studied the dynamics of internal waves in a stratified lake in response to the seasonal variations in the stratification and in wind characteristics. We conducted high-resolution observations in the Dead Sea, throughout the stratification season (May to December 2012), including high-resolution temperature profiling with a fiber optic system as well as lake level and wind measurements. A series of three-dimensional model simulations were conducted to analyze the internal waves and their variations with seasonal changes of stratification and wind.

We found a high correlation between the vertical fluctuations of the thermocline depth and the lake level. The correlation coefficient closely follows the observed density ratio between the water layers, corresponding to a two layer model maintaining hydrostatic pressure. The largest fluctuations appear during early spring and late fall, when stratification is relatively weak,

whereas moderate fluctuations occur in mid-summer when the stratification is fully developed. Upon considering the interannual changes of the lake's stability due to anthropogenic diversions of water from the Dead Sea basins over the past four decades, we identified increasing amplitudes and periods (i.e., lower frequencies) of the internal waves.

Measurements of the lake level and thermocline depth conducted at a number of locations in the lake provided insight on the spatial propagation of the surface and the internal waves. The model reproduced the observed propagation direction and speed of the dominant first baroclinic mode.

Spectral analyses of the wind, lake level, and thermocline depth show a very pronounced diurnal wind cycle during summer that is also expressed as a forced response of the surface waves. During spring and fall, a hint of longer period modes (~1.5 and 3 d, respectively) appears in the wind in addition to the diurnal cycle. Consequently, the level and thermocline depth fluctuations power spectra show substantial response at relatively long periods, whereas the 24 h mode is weak or absent. Three-dimensional model simulations were conducted for studying the normal modes of the lake. The results showed mainly a long-period, subdiurnal response for the Dead Sea (~45 h in August and ~72 h in October with typical respective density differences) that closely agreed with the estimated phase speed of the first baroclinic mode. For the historical meromicitic period with a very large density difference, the period of the first internal mode is ~20 h.

The measurements and model analysis suggest that the lower frequency normal modes may be excited in the lake when the wind imparts some energy at longer, subdiurnal periods in addition to the typical diurnal frequency. Thus, for example, in the fall, when wind forcing contains some energy at frequencies close to those of the natural basin-scale internal waves, resonant amplification of the internal waves may occur.

Interestingly, concurrent with the internal waves pycnocline fluctuations, double diffusion salt fingering also acts across the pycnocline interface in the Dead Sea, effectively advecting heat and salt between the strata (Arnon et al. 2016). This phenomenon includes staircases of density at the interface that are likely to be affected by the internal waves fluctuations. A systematic study of the interactions between these phenomena, internal waves and diapycnal fluxes, requires numerical modeling in the scale of the salt fingers, which is beyond the scope of this article.

References

- Anati, D. A. 1997. The hydrography of a hypersaline lake, p. 89–103. *In* T. M. Niemi, Z. Ben-Avraham, and J. R. Gat [eds.], The Dead Sea—the lake and its setting. Oxford Univ. Press.
- Arnon, A., N. G. Lensky, and J. S. Selker. 2014*a*. High-resolution temperature sensing in the Dead Sea using fiber optics. Water Resour. Res. **50**: 1756–1772. doi:10.1002/2013WR014935

- Arnon, A., J. Selker, and N. Lensky. 2014*b*. Correcting artifacts in transition to a wound optic fiber: Example from high-resolution temperature profiling in the Dead Sea. Water Resour. Res. **50**: 5329–5333. doi:10.1002/2013WR014910
- Arnon, A., J. S. Selker, and N. G. Lensky. 2016. Thermohaline stratification and double diffusion diapycnal fluxes in the hypersaline Dead Sea. Limnol. Oceanogr. **61**: 1214–1231. doi:10.1002/lno.10285
- Blumberg, A. F., and G. L. Mellor. 1987. A description of a three-dimensional coastal ocean circulation model. Three-dimensional coastal ocean models **4**: 1–16. doi:10.1029/CO004p0001
- Forcat, F., E. Roget, M. Figueroa, and X. Snchez. 2011. Earth rotation effects on the internal wave field in a stratified small lake: Numerical simulations. Limnetica **30**: 27–42. doi:10.23818/limn.30.04
- Genin, A., B. Lazar, and S. Brenner. 1995. Vertical mixing and coral death in the Red Sea following the eruption of mount Pinatubo. Nature **377**: 507–510. doi:10.1038/377507a0
- Gertman, I., and A. Hecht. 2002. The Dead Sea hydrography from 1992 to 2000. J. Mar. Syst. **35**: 169–181. doi:10.1016/S0924-7963(02)00079-9
- Gertman, I., N. Kress, B. Katsenelson, and P. Zavialov. 2010. Equations of state for the Dead Sea and Aral Sea: Searching for common approaches. IOLR report IOLR/12/2010. Israel Oceanographic and Limnological Research.
- Hall, J. K. 1981. The MEDMAP project: A systematic analysis of eastern Mediterranean marine geophysical data, p. 89–94. *In* R. Bogoch [ed.], Geological Survey of Israel current research 1980. Geological Survey of Israel.
- Halpert, M. S., C. F. Ropelweski, T. R. Karl, J. K. Angell, L. W. Stowe, R. R. Heim, A. J. Miller Jr., and D. R. Rodenhuis. 1993. 1992 brings return to moderate global temperatures. Eos Trans. Am. Geophys. Union **74**: 433–439. doi:10.1029/93EO00372
- Hamdani, I., S. Assouline, J. Tanny, I. M. Lensky, I. Gertman, Z. Mor, and N. G. Lensky. 2018. Seasonal and diurnal evaporation from a deep hypersaline lake: The Dead Sea as a case study. J. Hydrol. 562: 155–167. doi:10.1016/j.jhydrol.2018.04.057
- Hecht, A., and I. Gertman. 2003. Dead Sea meteorological climate, p. 68–114. *In* E. Nevo, A. Oren, and S. P. Wasser [eds.], Fungal life in the Dead Sea. A.R.G. Ganter Verlag K.G.
- Horn, W., C. H. Mortimer, and D. J. Schwab. 1986. Wind induced internal seiches in Lake Zurich observed and modeled. Limnol. Oceanogr. **31**: 1232–1254. doi:10.4319/lo.1986.31.6.1232
- Lemmin, U., C. H. Mortimer, and E. Bäuerle. 2005. Internal seiche dynamics in Lake Geneva. Limnol. Oceanogr. **50**: 207–216. doi:10.4319/lo.2005.50.1.0207
- Lensky, I. M., and U. Dayan. 2012. Continuous detection and characterization of the sea breeze in clear sky conditions using Meteosat second generation. Atmos. Chem. Phys. **12**: 6505–6513. doi:10.5194/acp-12-6505-2012
- Lensky, N. G., Y. Dvorkin, V. Lyakhovsky, I. Gertman, and I. Gavrieli. 2005. Water, salt, and energy balances of the Dead Sea. Water Resour. Res. **41**: 1–13. doi:10.1029/2005WR004084

- Lensky, N. G., I. Gertman, A. Arnon, T. Ozer, E. Biton, B. Katsenelson, and R. Bodzin. 2013. Currents and hydrography of the Dead Sea: A study for the Salt Recovery Project. *Geol. Surv. Israel Rep. no.* GSI/20/2013, 31 p.
- Lensky, N. G., I. M. Lensky, A. Peretz, I. Gertman, J. Tanny, and S. Assouline. 2018. Diurnal course of evaporation from the Dead Sea in summer: A distinct double peak induced by solar radiation and Night Sea breeze. Water Resour. Res. **54**: 150–160. doi:10.1002/2017WR021536
- Mellor, G., and A. Blumberg. 2004. Wave breaking and ocean surface layer thermal response. J. Phys. Oceanogr. **34**: 693–698. doi:10.1175/2517.1
- Mellor, G. L., and T. Yamada. 1982. Development of a turbulence closure model for geophysical fluid problems. Rev. Geophys. **20**: 871–875. doi:10.1029/RG020i004p00851
- Mor, Z., S. Assouline, J. Tanny, I. M. Lensky, and N. G. Lensky. 2018. Effect of water surface salinity on evaporation: The case of a diluted buoyant plume over the Dead Sea. Water Resour. Res. **54**: 1460–1475. doi:10.1002/2017WR021995
- Mortimer, C. H. 1953. The resonant response of stratified lakes to wind. Schweizerische Zeitschrift Hydrol. **15**: 94–151. doi: 10.1007/BF02486219
- Mortimer, C. H. 1993. Long internal waves in lakes: Review of a century of research. Center for Great Lakes Studies. Special Report 42.
- Rozas, C., A. de la Fuente, H. Ulloa, P. Davies, and Y. Niño. 2014. Quantifying the effect of wind on internal wave resonance in Lake Villarrica, Chile. Environ. Fluid Mech. **14**: 849–871. doi:10.1007/s10652-013-9329-9
- Sade, A. R., and others. 2014. Multibeam Bathymetric Map of the Dead Sea, Geological Survey of Israel report GSI/01/2014, Jerusalem, Israel.
- Schwab, D., and D. Beletsky. 2003. Relative effects of wind stress curl, topography, and stratification on large-scale circulation in Lake Michigan. J. Geophys. Res.: Oceans **108**: 3044. doi:10.1029/2001JC001066
- Selker, J. S., and others. 2006. Distributed fiber-optic temperature sensing for hydrologic systems. Water Resour. Res. **42**: W12202. doi:10.1029/2006wr005326
- Sirkes, Z., F. Schirmer, H. H. Essen, and K. W. Gurgel. 1997. Surface currents and seiches in the Dead Sea, p. 104–113. *In* T. M. Niemi, Z. Ben-Avraham, and J. R. Gat [eds.], The Dead Sea—the Lake and its setting. Oxford Univ. Press.
- Sirota, I., A. Arnon, and N. G. Lensky. 2016. Seasonal variations of halite saturation in the Dead Sea. Water Resour. Res. **52**: 7151–7162. doi:10.1002/2016WR018974
- Sirota, I., Y. Enzel, and N. G. Lensky. 2017. Temperature seasonality control on modern halite layers in the Dead Sea: In situ observations. GSA Bull. **129**: 1181–1194. doi:10.1130/B31661.1

- Steinhorn, I. 1991. On the concept of evaporation from fresh and saline bodies. Water Resour. Res. **27**: 645–648. doi: 10.1029/90WR02759
- Stiller, M., J. R. Gat, N. Bauman, and S. Shasha. 1984. A short meromictic episode in the Dead Sea: 1979–1982. SIL Proc. 1922–2010 **22**: 132–135. doi:10.1080/03680770.1983.11897279
- Tyler, S. W., J. S. Selker, M. B. Hausner, C. E. Hatch, T. Torgersen, C. E. Thodal, and S. G. Schladow. 2009. Environmental temperature sensing using Raman spectra DTS fiber-optic methods. Water Resour. Res. 45: W00D23. doi: 10.1029/2008wr007052
- Vercauteren, N., H. Huwald, E. Bou-Zeid, J. S. Selker, U. Lemmin, M. B. Parlange, and I. Lunati. 2011. Evolution of superficial lake water temperature profile under diurnal radiative forcing. Water Resour. Res. 47: W09522. doi:10.1029/2011wr010529
- Watson, E. R. 1904. Movements of the waters of loch ness, as indicated by temperature observations. Geogr. J. **24**: 430–437. doi:10.2307/1775951
- Wedderburn, E. M. 1912. Investigation of temperature distribution in Loch Earn. Scott. Geogr. Mag. **28**: 76–89. doi: 10.1080/14702541208555104
- Weinstein, R., N. Paldor, D. A. Anati, and A. Hecht. 2000. Internal seiches in the strongly stratified Dead Sea. Isr. J. Earth Sci. **49**: 45–53.
- Williams, W. D. 2001. Anthropogenic salinisation of inland waters. Hydrobiologia **466**: 329–337. doi:10.1023/A:1014598509
- Wyrtki, K., and R. Kendall. 1967. Transports of the Pacific equatorial countercurrent. J. Geophys. Res. **72**: 2073–2076. doi:10.1029/JZ072i008p02073

Acknowledgments

Two anonymous reviewers, Craig Stevens (Associate Editor), and Editor Robert Howarth are acknowledged for their constructive reviews of the manuscript. We are in debt to Raanan Bodzin, Hallel Lutzky, Tal Ozer, Boris Katsenelson, Assaf Mor, Ziv Mor, and Hagai Eyal for their dedicated intensive field and laboratory assistance. The R/V *Taglit* team, Silvy Gonen, Shahar Gan-El, and Meir Yifrach, operated the R/V under the harsh conditions of the Dead Sea; without them this research would not have been completed. This study was supported by the Israeli Government under Geological Survey of Israel Dead Sea Project 40391 and by the Israel Science Foundation grant 1471/18 (PI NL).

Conflict of Interest None declared.

Submitted 22 June 2018 Revised 07 November 2018; 27 January 2019 Accepted 04 February 2019

Associate editor: Craig Stevens